Structural Features and Molecular Assembly of Amorphous Phosphazenic Materials in the Bulk—Combined Theoretical and Experimental Techniques: Tris-(2,2′-dioxy-1,1′-binaphthyl)cyclotriphosphazene

Maria E. Amato,[a] Ruggero Caminiti,[b] Gabino A. Carriedo,[c] Francisco J. Garcia-Alonso,[c] Jose L. García-Alvarez,[c] Giuseppe M. Lombardo,[a] and Giuseppe C. Pappalardo*[a]

Abstract: The structure and the assembly of tris-(2,2′-dioxy-binaphthyl)cyclotriphosphazene {(+)-[$N_3P_3(O_2C_{20}H_{12})_3$], DBNP, in the solid amorphous state was studied using molecular dynamics (MD) including ad hoc quantum mechanically derived force field (FF) parameters, in combination with the energy dispersive X-ray diffraction (EDXD) technique. The atom–atom radial distribution function (RDF) curve obtained through the EDXD experiment revealed low intensity peaks not attributable to the intramolecular distances of the single molecule, but clearly featuring a low energy state of long-distance three-dimensional assembly. The radial distribution functions (RDF) were calculated for various models of DBNP submitted to theoretical MD simulations. Based on the comparison of theoretically calculated RDFs and those obtained from the EDXD experiment, the predominant structural motif of the material in the bulk was found to have DBNP molecules laid one upon the other to form tubular nanostructures. These contain eight DBNP units each (length ca. 46 Å) with two and three of these units aligned in parallel and held together. The material can be represented as a bulk of tubular snake-like chains undergoing distortions with a step of eight DBNP units. The bending angles, that vary randomly, attain limited values sufficient to induce disorder and thus nonperiodic structure. The present application of MD simulations combined with EDXD data appear to be a general approach to solve for the first time otherwise intractable issues concerning structural features and assembly of molecular materials in the bulk.

Keywords: molecular dynamics · nanostructures · phosphazenes · solid-state structures · X-ray diffraction

Introduction

The chemistry of hexa(aryloxy)cyclotriphosphazenes $N_3P_3(OAr)_6$ has many aspects of interest[1] and has been the subject of comprehensive surveys.[2] The presence of one to three dioxy-aryl or other dinucleophilic substituent groups closing rings with the phosphorus atoms gives rise to the so-called spirocyclophosphazenes.[3, 4] These compounds are of special interest because they represent a unique class of highly tailorable host molecules.[5] In fact, the formation of inclusion compounds with small molecules,[6] or polymers,[5] and in some cases, the induction of polymerization of the guest,[7] and the formation of nanometer-sized particles[8] have been reported.

The solid-state structures and conformations of hexa(aryloxy)cyclotriphosphazenes bearing bulky aryloxy-groups have been previously studied by us using X-ray diffraction analysis.[9–11] The X-ray structural analyses of several spirocyclophosphazenes[12–15] and, recently, of some sulphur and/or oxygen-containing monospirofluorophosphazenes, have also been reported.[16]

Thus, all these data refer to structural and conformational properties in the crystal state. The structural characteristics and the molecular assembly in the bulk would remain quite unknown for amorphous cyclophosphazenes and spirocyclic phosphazenes unless suitable theoretical force-field computational and experimental techniques become applicable.

The present investigation focuses on the tris-(2,2′-dioxy-binaphthyl)cyclotriphosphazene ((+)-[$N_3P_3(O_2C_{20}H_{12})_3$], DBNP, Figure 1) as an appropriate structural model for the high

[a] Prof. G. C. Pappalardo, Dr. M. E. Amato, Dr. G. M. Lombardo
Dipartimento di Scienze Chimiche, Cattedra di Chimica Generale
Facoltà di Farmacia, Università di Catania
Viale A. Doria 6, 95125 Catania (Italy)
Fax: (+39) 95-337751
E-mail: gcpappalardo@dipchi.unict.it

[b] Prof. R. Caminiti
Istituto Nazionale per la Fisica della Materia
Dipartimento di Chimica, Università La Sapienza
p.le A. Moro 5, 00185 Roma (Italy)

[c] Prof. G. A. Carriedo, Prof. F. J. Garcia-Alonso, Dr. J. L. García-Alvarez
Departamento de Química Orgánica e Inorganica
Facultad de Química, Universidad de Oviedo
Oviedo 33071 (Spain)

0947-6539/01/0707-1486 $ 17.50+.50/0

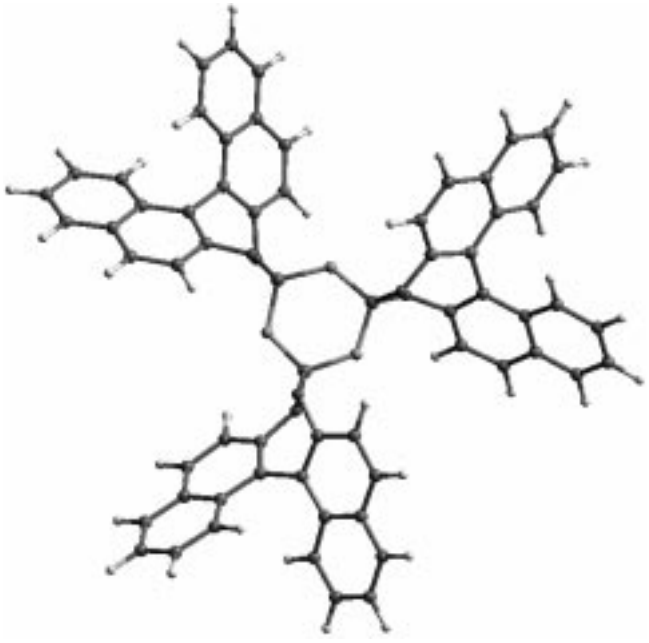

Figure 1. View of DBNP along the C_{3v} symmetry axis.

molecular weight chiral polyphosphazenes $[NP(O_2C_{20}H_{12})]_n$ described recently.[17, 18] Both the cyclic and polymeric chiral binaphthoxyphosphazenes have potential interest in enantiomeric separations or catalysis now under investigation.

The major impediment to understanding the structural features of DBNP is that it is an amorphous material. Wide-angle X-ray scattering (WAXS) is a powerful technique in the determination of structural parameters (interatomic distances) of amorphous systems[19, 20] since it can provide information on the short range order. In particular, energy dispersive X-ray diffraction (EDXD) has been recognised as a suitable tool in the investigation of such systems because of its speed and reliability compared with those of a traditional angular scanning diffractometer.[21–23] In our recent works[24, 25] the EDXD technique combined with molecular modeling and molecular dynamics (MD) was found be also suitable in providing information about the long-range order and thus allowed us to determine the backbone conformation of amorphous poly[bis(4-methylphenoxy)phosphazene] and semicrystalline poly[bis(phenoxy)phosphazene]. This approach has not yet been exploited for the determination of the structure, the occurrence and the extension of short range ordered portions in amorphous molecular materials.

The goals of this paper are therefore two-fold: first to provide additional experimental information about the structure of DBNP, its molecular assembly in the bulk (solid state), that is, its three-dimensional molecular order; and second to extend the use of computational chemistry combined with the EDXD technique for describing structural features of short-range ordered molecular materials that are amorphous in nature and are not amenable to single-crystal X-ray diffraction. Specifically, in this work we apply EDXD to derive the radial distribution function (RDF) from X-ray scattering data for DBNP. Molecular mechanics (MM) including ad hoc quantum mechanically derived force field (FF) parameters for CHARMm is used for modeling and predicting the RDF derived from the EDXD experiment. Verification of consistency between theoretical and experimental RDFs will allow atomic scale information on the structural situation of DBNP for each model considered, and in particular on the local order and short range interatomic distances. The local order refers to the intermolecular assembly of the DBNP units, to the alignment of the molecules, and/or to determine the structure of the preponderant nanostructured portions. To our knowledge this is the first report both on the molecular assembly in the bulk of an amorphous molecular material and on the structural characterization of such an extensively sterically crowded amorphous spirocyclic phosphazene.

X-ray Techniques

X-ray Experiments: The X-ray diffraction experiments described herein were carried out by employing a non-commercial X-ray energy scanning diffractometer[26, 27] equipped with an X-ray generator (water cooled, W target having 3.0 kW maximum power), solid-state detector (SSD) connected to a multichannel by means of an electronic chain collimator system, step motors and sample holder. The X-ray source is a standard Seifert tube (45 kV and 35 mA) with the white bremsstrahlung component being used. The necessary absorption corrections to combine the various angular data sets were made as described by Nishikawa and Iijima.[28, 29]

Radial distribution functions $D(r)$ were calculated from the static structure functions $i(q)$ [Eq. (1)]:

$$i(q) = I_{\mathrm{Coh}}(E,\theta) - \Sigma_n c_n f_n^2(q) \tag{1}$$

according to the expression:

$$D(r) = 4\pi r^2\rho_0 + 2r\pi^{-1}\int_0^{q_{\max}} qi(q)\sin(rq)dq \tag{2}$$

In this Equation $\rho_0 = (\Sigma_i n_i f_i(0))^2 V^{-1}$, V is the stoichiometric unit of the chosen volume, n_i = number of atoms "i" per unit volume, and f_i the scattering factor per atom "i". Symbols in Equations (1) and (2) are as defined previously.[26–29] As an upper integration limit for $q_{\max}$ we used 15.42 Å^{-1}.

X-ray Data analysis: To quantitatively assess the precise origins of the RDF our analysis of the experimental scattering data was made by comparing the theoretical RDFs produced by the MM and MD models considered in this work. The features of the RDF are determined by both the structural arrangement of a single molecule and the adopted packing structure by neighboring molecules. Two methods of analysis were used: the calculation of $i(q)$ by the single static models taking into consideration the fluctuation of the interatomic distances through the introduction of its rms variation by a σ_{jk} parameter, and calculation of $i(q)$ by obtaining the fluctuation of the distances by an MD run.

In the first case, the theoretical RDF peaks were calculated from the Fourier transform of the theoretical intensities for pairs of interactions [Eq. (3)].

$$i(q) = \Sigma f_j f_k \frac{\sin(r_{jk}q)}{r_{jk}q}\exp(-1/2\,\sigma_{jk}^2 q^2) \tag{3}$$

using the same scattering parameter interval (q) as for the experimental data and assuming the rms variations in the interatomic distance σ_{jk} to be constant in a set of ranges of interatomic distances. For each assumed structure model and related geometry the σ_{jk} values were optimized by best fit of the theoretical intensities (SF) to the experimental one.

The second method avoids the above assumption of static molecular arrangement involving the best fit of σ_{jk} values as empirically adjusted parameters. From MD simulations it is possible to calculate directly the RDF for every combination of atomic-type pairs (P···P, P···N, P···C, etc.), that is, $d_{nm}(r)$. Accordingly, the shape of the coherent scattering intensity curve was obtained through the RDF curves calculated from the snapshots collected along the entire evolution time of the simulation of each model. For this purpose the discrete sum of Equation (3) must be transformed into an integral expression in terms of the continuous pair distribution functions $d_{nm}(r)$ [Eq. (4)].

$$i(q) = \int_0^\infty 4\pi r^2 [f_P^2(q) c_P^2 d_{PP}(r) + f_P(q) f_N(q) c_P c_N d_{PN}(r) + \ldots] \frac{\sin(rq)}{rq} dr \qquad (4)$$

in which c_P, c_N, …, are the atomic concentrations in the chosen model. This allows the calculation of the theoretical intensity curve from a MD simulation.

In both cases, the $i(q)$ for the models were calculated disregarding the effects of the image atoms as a result of the periodic boundary conditions (PBC) used by the modeling procedure.

MD Simulations

Protocols: The Cerius[2] package developed by BIOSYM/MSI was used to perform all the MD calculations through the OFF (Open Force Field) routine that includes the empirical functions of the CHARMm force field.[30] The CHARMm FF parameters derived by us previously for hexa(aryloxy)cyclotriphosphazenes were used.[31] The Crystal facility of this program was used for reproducing the PBC, needed to avoid border effects. The atomic charges [P 0.512, N −0.113, O −0.504, C from −0.175 to 0.044, H from 0.099 to 0.138] were obtained with the charge equilibration method[32] implemented in the Cerius[2] package. The simulations were carried out using the NPT (constant pressure and temperature) and NVT (constant volume and temperature) ensembles, at $T = 298$ K started from energy-minimized structures obtained with the conjugate gradient method, satisfying a gradient ≤ 0.1 kJ mol^{-1} Å^{-1}.

The scale factor for the nonbonding (NB) 1–4 interactions was set to 0.5. The NB interactions cut-off was implemented according to the SPLINE method as a function of the interatomic distance values (r) as follows: for $r <$ SPLINE-ON = 10 Å, fully considered; for $r >$ SPLINE-OFF = 15 Å, fully ignored; for SPLINE-ON $< r <$ SPLINE-OFF, reduced in magnitude. The dielectric constant in the electrostatic function was set as $\varepsilon = 1$. Transients for 200 ps with sampling interval of 0.05 ps were usually collected. The integration time step was 0.001 ps.

Models: The first model (**M1**) to be considered was built up using 32 DBNP molecules randomly disposed within a box of $40 \times 40 \times 40$ Å. For the second model (**M2**) we assumed a crystalline order (one DBNP molecule per unit cell). The molecule was placed at the origin of the hexagonal cell ($a = b = 20$ Å, $c = 10$ Å, $\alpha = \beta = 90^\circ$ and $\gamma = 120^\circ$) which was deduced on the basis of the molecular size and symmetry (C_{3v}). The C_{3v} axis was set parallel to the c axis with two of the three N atoms directed towards a and b (Figure 2). This arrangement was chosen in order to obey to the condition of maximum distance of the DBNP molecule from the atoms of the image molecules. Various tests and trials performed through small manual modifications of the cell parameters and positioning of DBNP in the cell, followed by complete energy-minimization, by short MD runs, and again by energy-minimization, attained the optimized structure of **M2** (cell parameters: $a = 17.4$, $b = 17.8$, $c = 5.7$ Å, $\alpha = 90.5^\circ$, $\beta = 99.2^\circ$ and $\gamma = 120.2^\circ$). This cell was repeated along its c axis in order to generate the **M2-*n*** models that correspond to the tubular structures containing $n = 2-10$, 12, 14, and 16 DBNP units (Figure 2).

Modification of the **M2-*n*** models into **M3-ϕ** models was attained through relative rotations of adjacent molecules around the c axis, denoted by the angle value $\phi = 5$, 10, 15, 20, 30°, and subsequent readjustment of the lengths of the a and b axes to avoid contacts with the image molecules.

Additional pillared models **M2-*n*-*N*** having $N = 2$, 3 and 4 pillars were based on the **M2-*n*** models by duplicating the **M2-*n*** tubes along the a or b axis, or along both a and b axes. The models **M2-8-2/*a*** and **M2-8-2/*b***, duplicated along axis a and axis b, are shown in Figure 3a and 3b, respectively.

Sample: The DBNP sample (specific rotation: +70° in $CHCl_3$, $c = 0.5$) was prepared and purified as described elsewhere.[17] The purity was verified by elemental analysis and by NMR spectroscopy. The ^{13}C and ^1H NMR spectra in $CDCl_3$ were performed at 499.89 MHz on a Varian Unity Inova 500 spectrometer.

Results and Discussion

Figure 4 shows a) the observed structure function and b) the corresponding RDF in the range 0 to 80 Å. By considering that the maximum *intra*molecular distance falls within 17.5 Å, the RDF in the long-distances region (from ca. 20 to 80 Å) shows low intensity peaks not attributable to the intramolecular distances of the single molecule, but clearly featuring a very low state of molecular three-dimensional order. The NPT simulation of the fully disordered model **M1** provided theoretical curves in strong disagreement with the experimental ones (Figure 4a and b). Notably the RDF of **M1** shows: i) short distances peaks (<10 Å) that occur at the same position as the experimental ones, but having lower intensities; ii) in the long distance range, the periodicity of the calculated peaks is shifted with respect to experimental peaks. On these grounds, it can be argued that the solid DBNP should not be completely disordered, and that some degree of structural order is likely within the range of the intramolec-

0947-6539/01/0707-1488 $ 17.50+.50/0 *Chem. Eur. J.* **2001**, *7*, No. 7

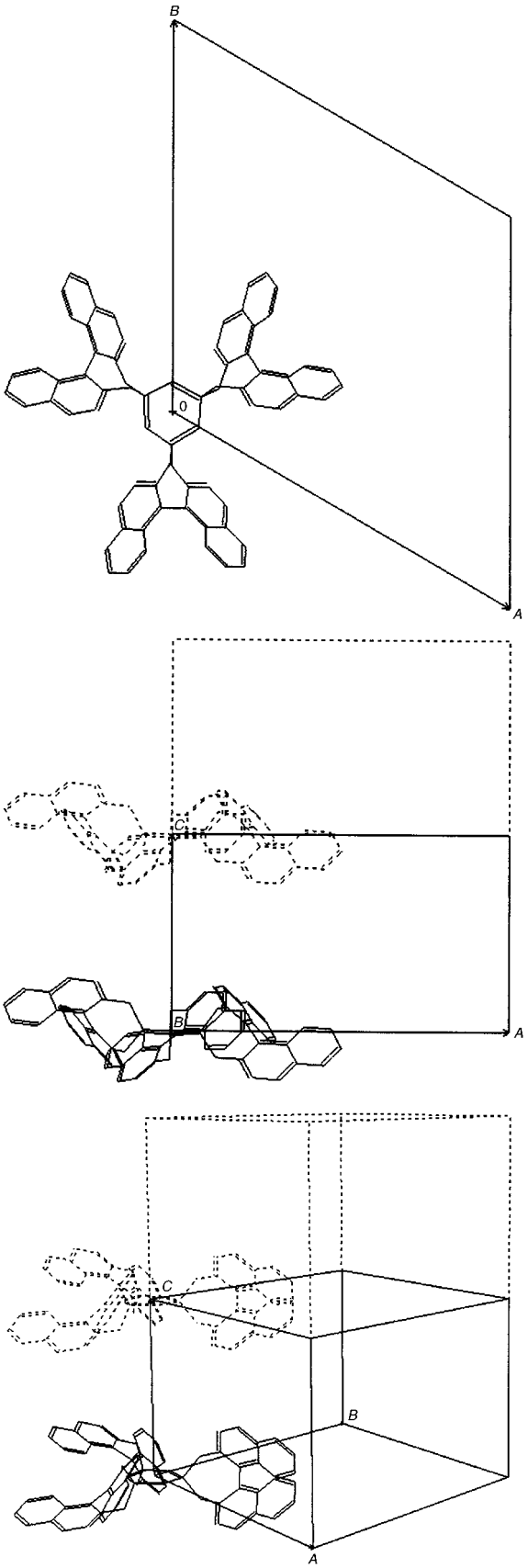

Figure 2. Construction of M2-type models in the assumed hexagonal unit: a) view of the *ab* plane (the mass center of DBNP molecule is positioned at the origin of the axes); b) view of the *ac* plane; c) a perspective view of the model. Dotted line drawing denotes duplication step along the *c* axis of the DBNP unit. Hydrogen atoms were omitted for sake of clearness.

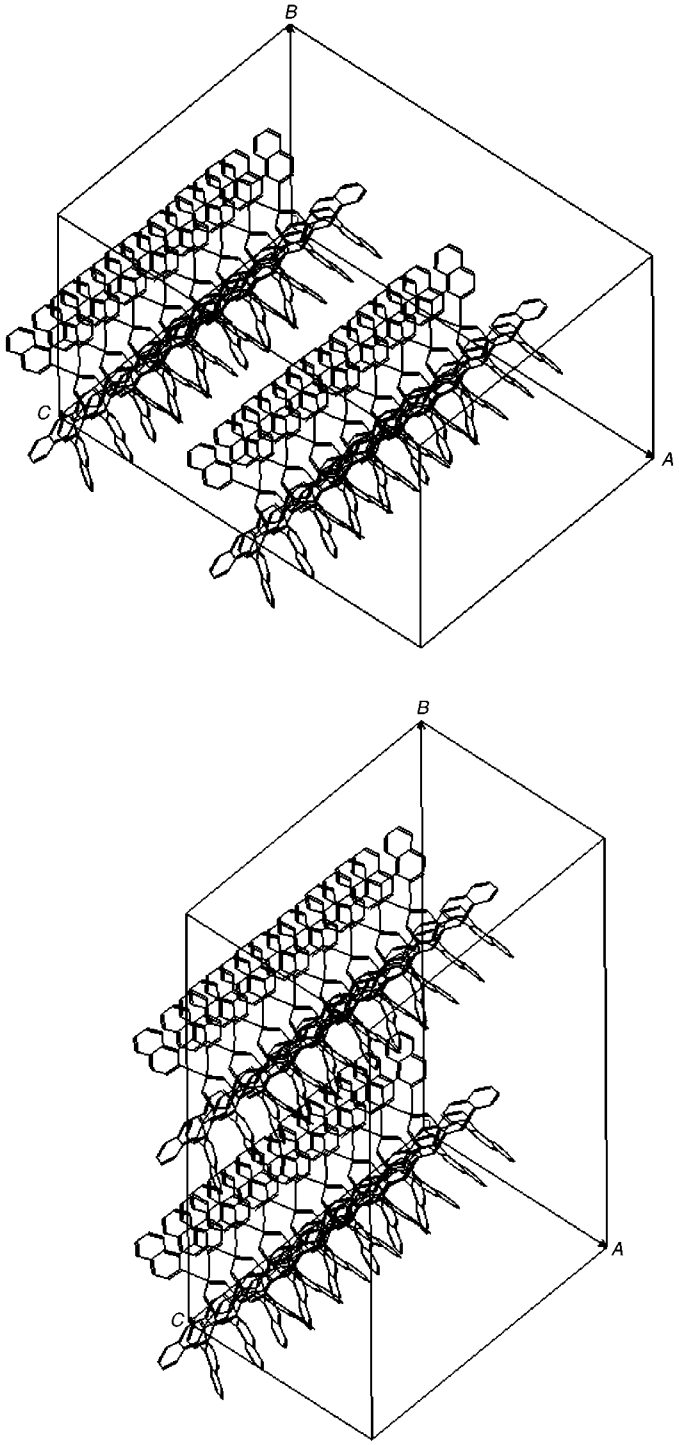

Figure 3. View of the models a) **M2-8-2/*a*** and b) **M2-8-2/*b*** in which the different relative positioning along *a* and *b* axes are outlined.

ular distances (0–15 Å). This was confirmed by better results from MD simulations of the **M2** models in their various extensions. Figure 5 shows comparisons between measured and calculated RDFs from NVT MD simulations of the selected **M2-8-2** and **M2-8-3** models with the columns aligned in the directions of *a* or *b*. Among the whole set of **M2** type models having tubular structures made by a variable numbers n of DBNP units and N of pillars, those in which $n = 8$ and

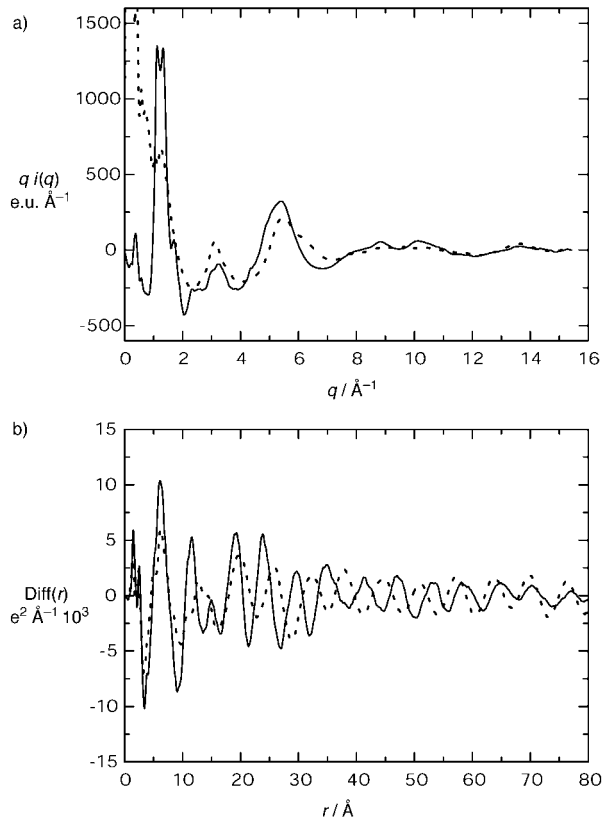

Figure 4. Comparison between experimentally (EDXD) observed (solid line), and a) MD calculated (dotted lines) structure function and b) related RDF for the model **M1**.

$N = 2$, 3 gave the RDF best reproducing the experimental results. The peaks ranging from 0 to about 18 Å agree quite well with the theoretical ones for models **M2-8-2/*a*** (rmsd[33] = 0.95) and **M2-8-3/*a*** (rmsd = 0.99) (Figure 5a and c). In the range 19–40 Å the calculated RDFs (rmsd = 2.94 and 3.98, respectively) do not match so well the positions and the lower intensities of the experimental peaks, thus suggesting that the extension of the order in these models is greater than that of the DBNP in the bulk. The calculated peaks agree well enough with the experimental ones from 0 up to 40 Å in the case of the **M2-8-2/*b*** (rmsd = 1.45) and **M2-8-3/*b*** (rmsd = 1.75) models (Figure 5b and d). The positions of the peaks at about 14 and 18 Å are well centred, but their intensities are relatively higher than the experimental ones. Beyond 40 Å these models are not suitable as a result of their limited lengths (*c* axis being about 46 Å).

To safely check that the observed slight differences between calculated **M2** type models and experimental RDFs were independent of the assumed period along the ordered tubular structure, the **M3-**ϕ type models, in which adjacent molecules were rotated around their C_{3v} axis by angle steps of $\phi = 5°$, 10°, 15°, 20°, 30°, were simulated and their RDFs calculated. All models attained a spiral shape structure featured by a longer period along the *c* axis, and by intermolecular distances different from those of the **M2**-type models. All the RDFs calculated for the **M3-**ϕ models overlap well up to 10 Å of the experimental, and are featured by the absence of the peak at about 15 Å and by shifted periodicity of the calculated peaks from 25 Å. The model **M3-8-2/*b*/**$\phi = 15°$ case is shown in

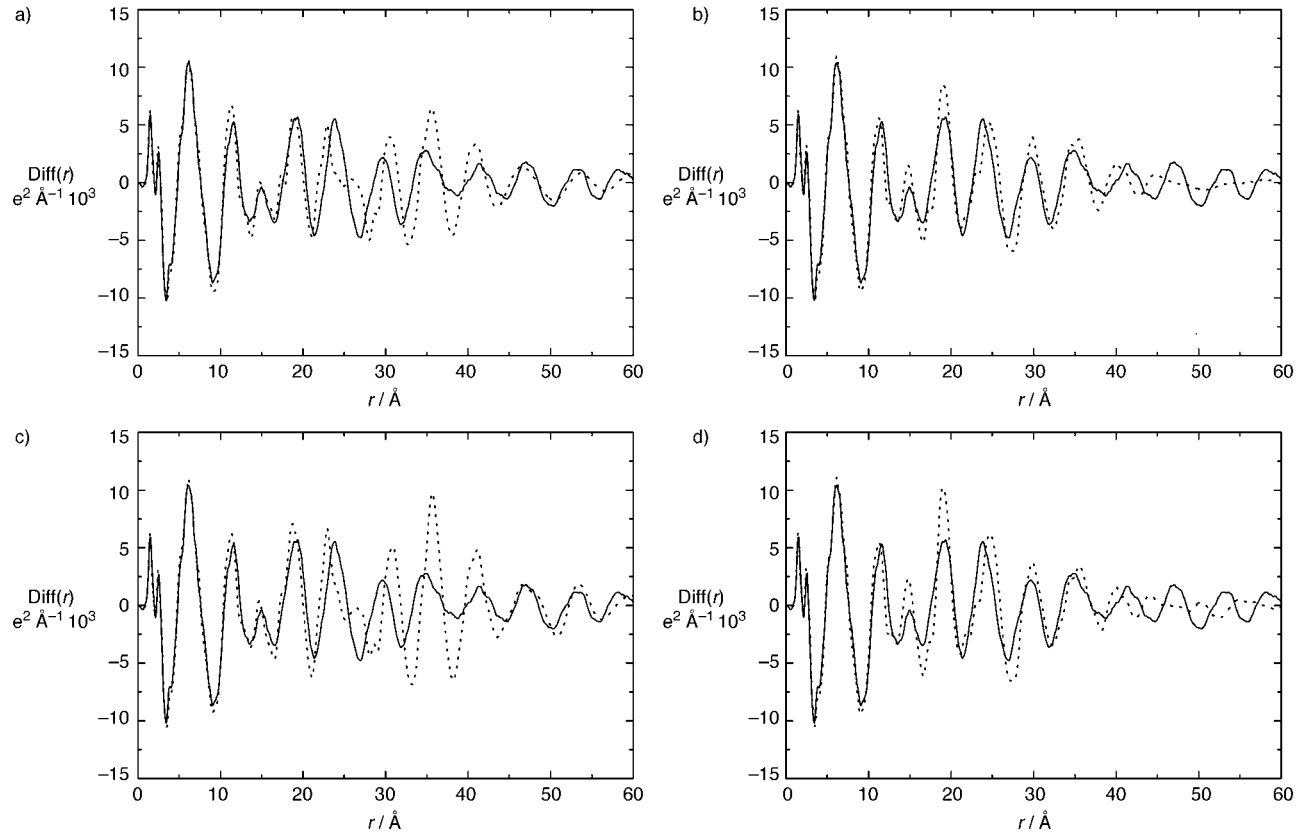

Figure 5. Comparison between experimentally (EDXD) observed (solid line), and MD calculated (dotted line) RDFs for the models a) **M2-8-2/*a***, b) **M2-8-2/*b***, c) **M2-8-3/*a***, d) **M2-8-3/*b***.

0947-6539/01/0707-1490 $ 17.50+.50/0 *Chem. Eur. J.* **2001**, *7*, No. 7

Figure 6. On the basis of these results, the latter spiral-shaped models can be ruled out.

The **M2-16-2** model, that is two columns of 16 molecules each, was submitted to MD runs in the gas phase with the aim to attain wider fluctuations than in the cases in which the PBC

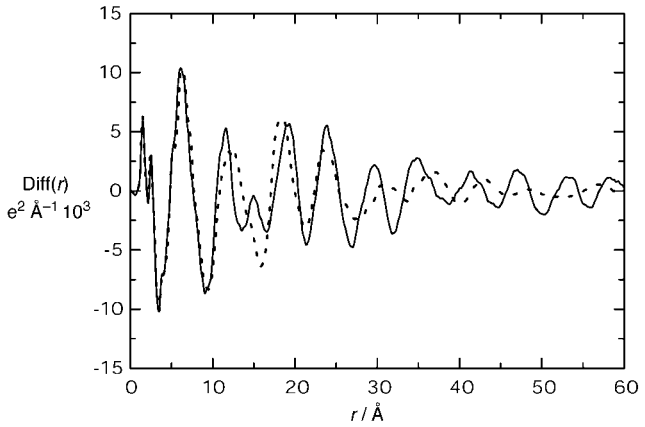

Figure 6. Comparison between experimentally (EDXD) observed (solid line), and MD calculated (dotted lines) RDF for model **M3-8-2/*b*/**$\phi = 15°$.

are applied, and accordingly to simulate the degree of disorder needed to reproduce the long distance portion of the experimental RDF.

A simulation in the gas phase[34] of the **M2-16-2** model resulted in the unique RDF model (rmsd = 0.46) in the range 40–80 Å which is compatible with the experimental model (Figure 7), and thus suited to give a good insight into the long

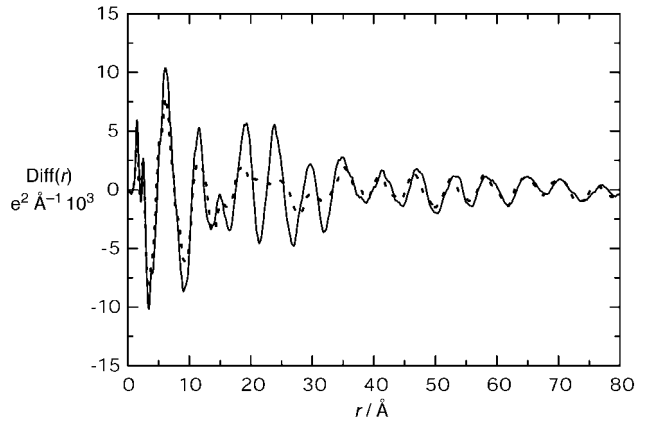

Figure 7. Comparison between experimentally (EDXD) observed (solid line), and MD calculated (dotted line) RDF for the model **M2-16-2/*b*** in the gas phase.

-range disorder of the system. However, the shape of this calculated RDF from 0 up to 40 Å is in significant disagreement with that coming from the EDXD experiment. The best reproduction of the experimental RDF in the range of 0–40 Å was attained through **M2-8-2** and **M2-8-3** models as reported above, in which the length of the eight molecular units of DBNP pillars is about 46 Å. But interestingly, a snapshot of the MD simulations on the **M2-16-2** model collected at 50 ps showed that this model consists of two paired pillars of 16 DBNP units evolving to a spiral-like structure, and attains discontinuity and bending into two paired tubular fragments of eight molecules each (Figure 8).

The limited snake-like fluctuations of these fragments give an idea of how the material behaves in the bulk. One arrangement can be determined in which predominate, long-paired, tubular substructures are found (which maintain a

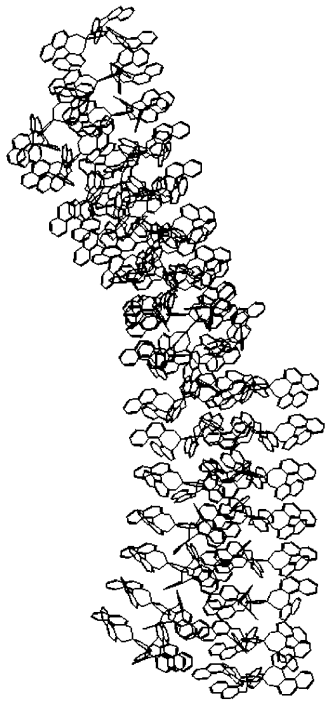

Figure 8. View of a snapshot (at 50 ps) of the MD simulation in the gas phase of the model **M2-16-2/*b***, showing the bending and discontinuity at the limit of the eight molecules portion structural motif.

local structural order up to about eight molecular units) with limited bending possibility with respect to each other. The system fluctuates in order to perform these bending processes of the eight molecular units tubes during the gas-phase MD trajectories. In the solid these bending processes are extremely slow, and therefore the distribution of the bending angles assumed by the DBNP tubular portions are retained. This distribution of angles inserts a degree of disorder sufficient to account for the amorphous state of DBNP in the solid. The results of this gas phase MD simulation thus add further support to the view of a predominant ordered arrangement of DBNP in the bulk as represented by the **M2-8** type models.

The other variations of the **M2-*n*** type models, which are possible by stacking two or more tubes together with different spatial orientations (rotation of one tube with respect to the first, shortening of one tube, and so on) were ruled out because all the calculated RDFs were not compatible with the experimental results.

Table 1 reports the average total energy per DNBP molecule in selected models. The data show that the energy of a single DBNP molecule in the gas phase is significantly higher ($\Delta_{(DBNP,M1)} = 122\ kJ\,mol^{-1}$) than the energy per molecule in the **M1**-, **M2**- and **M3**-type models. The energy of DBNP in the fully disordered model **M1** is higher than that in

Table 1. Averaged energies (E in kJ mol^{-1}) per DBNP units of selected models calculated by MD. The calculated energy for the isolated DBNP molecule in the gas phase is also given.

Energy	DBNP	**M1**	**M2-8-2/*a***	**M2-8-2/*b***	**M2-8-3/*a***	**M2-8-3/*b***	**M3-8-2/*b***
total	807.39	684.21	589.37	595.48	590.53	595.76	644.88
nonBonding	− 231.50	− 376.31	− 443.90	− 438.63	− 442.55	− 438.53	− 404.20
valence	1038.85	1060.52	1033.26	1034.11	1033.09	1034.29	1049.07

the remaining more ordered models ($\Delta_{(M1,M3)} = 40$, $\Delta_{(M3,M2)} = 50$ kJ mol^{-1}). Among these latter systems, the **M2** models are energetically more favored than the **M3** models which have a different structural order. This energy-based prediction is consistent with the representation of the material, in which the BDNP adopts a locally ordered molecular arrangement in the solid along a motif corresponding to the **M2**-type models.

Further support for the **M2** models is provided by the results of the data analysis of static models accomplished by an optimization procedure of the rms variations of the interatomic distances (σ_{jk} values) through best fit of the theoretical intensities $i(q)$ to the experimental values as described in the Section on X-ray data analysis. The final values of σ_{jk} obtained for the selected models **M2-8-2/*a*** and **M2-8-2/*b*** (Figure 9) are quoted in Table 2. These theoretical

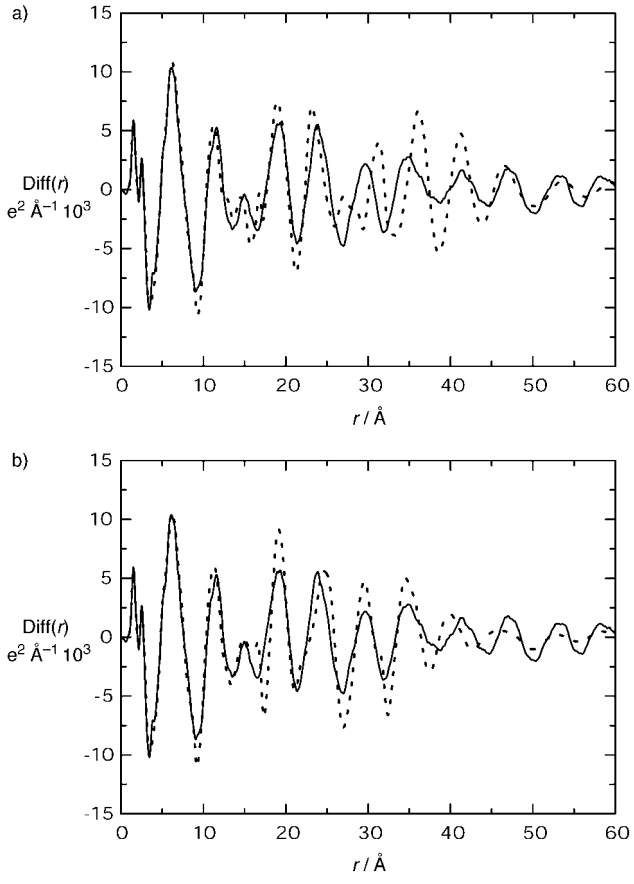

Figure 9. Comparison between experimentally (EDXD) observed (solid line) and calculated (dotted line) RDF assuming static models and optimization of the σ_{jk} values by best fit of the calculated intensities to the experimental intensities for the models a) **M2-8-2/*a*** and b) **M2-8-2/*b***.

Table 2. Final values of the adjusted σ_{jk} parameters for models I) **M2-8-2/*a*** and II) **M2-8-2/*b*** at various ranges of the interatomic distance (r).

Distance	σ_{jk} (I)	σ_{jk} (II)	Distance	σ_{jk} (I)	σ_{jk} (II)
$0.0 < r \leq 2.0$	0.088	0.087	$9.0 < r \leq 17.0$	0.212	0.224
$2.0 < r \leq 3.0$	0.138	0.134	$17.0 < r \leq 32.0$	0.281	0.320
$3.0 < r \leq 9.0$	0.175	0.170	$32.0 < r$	0.351	0.400

RDFs for the static models agree rather well with the corresponding calculated values through MD runs (Figure 5a and b), except for small differences (prediction of addition peak at ca. 17.5 Å). The additional calculated peaks detectable in Figure 9 are in fact inherent to the fitting procedure, which assumes constant σ_{jk} along wide intervals of the distance. The fitted σ_{jk} values change as a function of the distance with the same trend of the σ_{jk} obtained using MD trajectories of the same models. But in the case of some atom-type pairs the σ_{jk} values calculated by the MD simulations vary greatly for small variations of the distance, as outlined in Figure 10 though in a discontinuous fashion.

The interatomic distances of the DBNP molecule fall in the interval from 1.50 to about 18 Å of the experimental RDF (peaks: 1.50, 2.50, 6.10, 11.65, 14.95, 19.15 Å). In this region the MD calculated RDF curves for the models considered are in good agreement with the experimental curves, so that safe structural data of the molecule can be obtained from analysis of the MD trajectories. Table 3 reports the averaged interatomic distances and angles of a DBNP unit obtained over the entire evolution time of the **M2-8-2/*b*** model. The calculated bond lengths and angles are consistent with the experimental data (averaged values) of the analogous biphenyl-derivative tris-(2,2′-dioxybiphenyl)cyclotriphosphazene (DBPP) in the crystal.[14] The greater value for the C–C inter-ring bond length in DBNP compared with DBPP (by 0.05 Å) can be attributed to increased steric repulsion due to the larger naphthyl groups in DBNP; this results in distortion of the angle between the two naphthyl planes and consequently to elongation of the C–C inter-ring bond.

Conclusion

We have studied the amorphous DBNP in order to provide information about the structural features and the molecular arrangement in the bulk using in complementary fashion the EDXD experiment and computational chemistry (MD simulations). From our studies we find that: 1) the amorphous

0947-6539/01/0707-1492 $ 17.50+.50/0 *Chem. Eur. J.* **2001**, *7*, No. 7

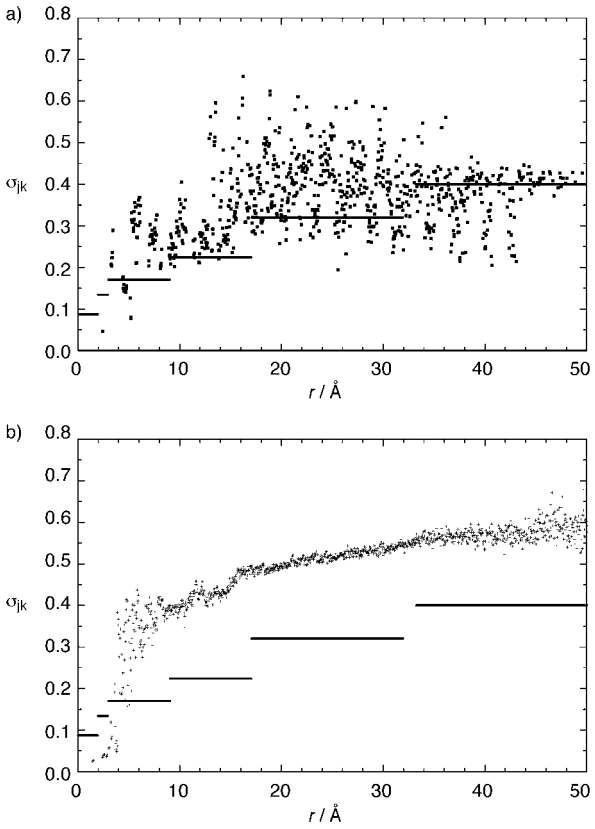

Figure 10. Comparison of the variation of the σ_{jk} values as a function of the distances, as monitored by the MD time evolution (dots), and as calculated by the fitting procedure (lines). Two atom types a) O···O and b) C···C are illustrated for the static model **M2-8-2/*a***.

Table 3. Comparison of average bond lengths (Å) and angles (*deg*) for DBNP[a] and tris-(2,2′-dioxyphenyl)cyclotriphosphazene (DBPP).[b]

	DBNP	DBPP		DBNP	DBPP
P–N	1.616	1.572	N-P-N	114.01	118.4
P–O	1.568	1.584	P-N-P	125.68	121.0
O–C	1.411	1.399	O-P-O	103.15	102.7
C–C[c]	1.528	1.478	N-P-O	109.73	108.6
C–C[d]	1.401	1.392	P-O-C	121.54	120.0
N-P-N-P	±3.33	±8.52			
P-N-P-O	±123.64	±124.61			
(O)C-C-C-C(O)	±53.14	±42.04[e]			

[a] This work. [b] X-ray crystal data ref. [14]. [c] Binaphthyl (DBNP) and biphenyl (DBPP) C–C bonds. [d] Aromatic C–C bonds within the naphthyl (DBNP) and phenyl (DBPP) groups.

DBNP is featured by a state of three-dimensional order; 2) the sample of PBPP studied shows a small ordered domain which can be represented by DBNP molecules laid one upon the other to form tubular structures of eight DBNP units each (length ca. 46 Å); 3) portions formed by two and three of these ordered tubular structures, aligned in parallel and held together, are the predominant structural motif in the material; 4) in general the material can be pictured as a bulk of long tubular chains of DBNP with a random, limited bending angle occurring with a step of eight DBNP units; 5) application of MD simulations, using suitable force field parameters, combined with EDXD data appears to be a general approach for solving otherwise intractable issues concerning structural features of molecular materials which are amorphous in nature and not amenable to single crystal X-ray diffraction. The proposed model should be considered a structural motif that might be recognized within the real structure in a more or less distorted form.

Acknowledgements

This work was supported by MURST of Italy.

[1] R. De Jaeger, M. Gleria, *Prog. Polym. Sci.* **1998**, *23*, 179–276.
[2] C. W. Allen, *Coord. Chem. Rev.* **1994**, *130*, 137–173.
[3] H. R. Allcock, U. Diefenbach, S. R. Pucher, *Inorg. Chem.* **1994**, *33*, 3091–3095.
[4] R. A. Pelc, K. Brandt, Z. Jedlinski, *Phosphorus, Sulfur Silicon* **1990**, *47*, 375–382.
[5] H. R. Allcock, A. P. Primrose, N. J. Sunderland, A. L. Rheingold, I. A. Guzei, M. Parvez, *Chem. Mater.* **1999**, *11*, 1243–1252.
[6] A. Comotti, M. C. Gallazzi, R. Simonutti, P. Sozzani, *Chem. Mater.* **1998**, *10*, 3589–3596.
[7] H. R. Allcock, E. N. Silverberg, G. K. Dudley, S. R. Pucher, *Macromolecules* **1994**, *27*, 7550–7555.
[8] T. Kobayashi, S. Isoda, K. Kubono, *Cyclophosphazenes*: *Structures and Molecular Selectivities*, in *Comprehensive Supramolecular Chemistry*, *Vol. 6* (Eds.: D. D. MacNicol, F. Toda, R. Bishop), Elsevier, Oxford, UK, **1996**, pp. 399–419.
[9] G. Bandoli, U. Casellato, M. Gleria, A. Grassi, E. Montoneri, G. C. Pappalardo, *Z. Naturforsch.* **1989**, *44b*, 575–581.
[10] G. Bandoli, U. Casellato, M. Gleria, A. Grassi, E. Montoneri, G. C. Pappalardo, *J. Chem. Soc. Dalton Trans.* **1989**, 757–750.
[11] G. Bandoli, M. Gleria, A. Grassi, G. C. Pappalardo, *J. Chem. Res.* (*S*) **1992**, 148–149.
[12] H. R. Allcock, R. W. Allen, E. C. Bissell, L. A. Smeltz, M. Teeter, *J. Am. Chem. Soc.* **1976**, *98*, 5120–5125.
[13] C. Combes-Chamalet, H.-J. Cristau, M. McPartlin, F. Plénat, I. J. Scowen, T. M. Woodroffe, *J. Chem. Soc. Perkin Trans. 2* **1997**, 15–18.
[14] H. R. Allcock, M. T. Stein, J. A. Stanko, *J. Am. Chem. Soc.* **1971**, *93*, 3173–3178.
[15] I. Dez, J. Levalois-Mitjaville, H. Grützmacher, V. Gramlich, R. De Jaeger, *Eur. J. Inorg. Chem.* **1999**, 1673–1684.
[16] A. Vij, S. J. Geib, R. L. Kirchmeier, J. M. Shreeve, *Inorg. Chem.* **1996**, *35*, 2915–2929.
[17] G. A. Carriedo, F. J. Garcia Alonso, P. A. Gonzalez, J. L. Garcia-Alvarez, *Macromolecules* **1998**, *31*, 3189–3196.
[18] G. A. Carriedo, F. J. Garcia Alonso, P. Gómez Elipe, J. L. García Alvarez, M. P. Tarazona, M. T. Rodriguez, E. Saiz, J. T. Vazquez, J. I. Padrón, *Macromolecules* **2000**, *33*, 3671–3679.
[19] R. Caminiti, C. Munoz Roca, D. Beltran Porter, A. Rossi, *Z. Naturforsch.* **1988**, *43a*, 591–596.
[20] D. Atzei, R. Caminiti, C. Sadun, R. Bucci, A. Corrias, *Phosphorus, Sulfur Silicon Relat. Elem.* **1993**, *79*, 13–24.
[21] T. Egami, H. J. Gunterodt, H. Beck, *Glassy Metals*, *Vol. 1*, Springer, Berlin, **1981**, pp. 25–61.
[22] A. Capobianchi, A. M. Paoletti, G. Pennesi, G. Rossi, R. Caminiti, C. Ercolani, *Inorg. Chem.* **1993**, *3*, 4635–4640.
[23] D. Atzei, D. De Filippo, A. Rossi, R. Caminiti, C. Sadun, *Spectrochim. Acta* **1995**, *51*, 11–20.
[24] R. Caminiti, M. Gleria, K. B. Lipkowitz, G. M. Lombardo, G. C. Pappalardo, *J. Am. Chem. Soc.* **1997**, *119*, 2196–2204.
[25] R. Caminiti, M. Gleria, K. B. Lipkowitz, G. M. Lombardo, G. C. Pappalardo, *Chem. Mater.* **1999**, *11*, 1492–1497.
[26] R. Caminiti, C. Sadun, V. Rossi, F. Cilloco, R. Felici, *XXVth Italian Congress of Physical Chemistry*, **1991**, Cagliari (Italy).
[27] R. Caminiti, C. Sadun, V. Rossi, F. Cilloco, R. Felici, *I. Patent RM/93 01261484*, **1993**.

[28] K. Nishikawa, T. Iijima, *Bull. Chem. Soc. Jap.* **1984**, *57*, 1750–1759.
[29] G. Fritsch, D. A. Keimel, *J. Mater. Sci. Eng. A* **1991**, *134*, 888–891.
[30] B. R Brooks, R. E. Bruccoleri, B. D. Olafson, D. J. States, S. Swaminathan, M. Karplus, *J. Comput. Chem.* **1983**, *4*, 187–217.
[31] M. E. Amato, K. Lipkowitz, G. M. Lombardo, G. C. Pappalardo, *J. Mol. Struct.* **1995**, *372*, 69–84.
[32] A. K. Rappe, W. A. Goddard III, *J. Phys. Chem.* **1991**, *95*, 3358–3363.
[33] The better quality of agreement can be obtained by the root mean square deviation (rmsd) for the RDF defined by the following Equation:

$$\mathrm{rmsd}_{\mathrm{RDF}} = \sqrt{\sum_{j}^{N} (\mathrm{RDF}_j^{\mathrm{exp}} - \mathrm{RDF}_j^{\mathrm{calcd}})^2 / N}$$

where N is the number of points generating the curve.
[34] In the assumed gas phase the codes /***a*** and /***b*** do not apply to denote the model, because the system is free from ties, so that the model may achieve whatever relative positioning of the "tubes".

Received: June 19, 2000 [F2551]

0947-6539/01/0707-1494 $ 17.50+.50/0